Journal of Natural Sciences Research
ISSN 2224-3186 (Paper) ISSN 2225-0921 (Online)
Vol.3, No.9, 2013

Voltage Curve for Annihilation Dynamics of A Vortex-Antivortex Pair in Mesoscopic Superconductor

Hari Wisodo[1, 2*], Pekik Nurwantoro[1], Agung Bambang Setio Utomo[1]
1. University of Gadjah Mada (UGM), Jl. Bulaksumur, Yogyakarta 55281, Indonesia
2. State University of Malang, Jl. Semarang 5, Malang 65145, Indonesia
* E-mail of the corresponding author: hariwisodo@gmail.com

Abstract
The voltage curve of the annihilation dynamics of a vortex-antivortex (VAV) pair in a mesoscopic superconductor has been investigated based on the Time Dependent Ginzburg Landau (TDGL) equations. The pair was generated only by the current-induced magnetic field. The influence of the annihilation dynamics of a VAV pair on the voltage curve is studied. As the external current density is passed on the sample, a VAV enters the scene, moves toward the centre of the sample, and finally the pair is annihilated. The position, velocity, and acceleration of the vortex and antivortex were calculated as a function of time. The supercurrent density topology, order parameter topology, and voltage curve were also calculated. The influence of the annihilation dynamics of a VAV pair on the voltage curve is discussed.
Keywords: annihilation, anti vortex, superconductor, vortex, voltage

1. Introduction

A vortex dynamics in a type-II superconductor may affect decreasing superconductivity of the superconductors. One of the trigger of the vortex movement is a current I passed on a superconductor. The influence of the vortex dynamics on the current-voltage characteristic V-I in a type-II superconductor have paid attention from researchers. Vodolazov and Peeters (2007) showed the influence of the vortex dynamics on the V-I characteristic curve. A pinning potential (Winiecki and Adam, 2002b) or defect (Machida and Kaburaki, 1994) on a type-II superconductor causes the slow increasing of the voltage V by the increasing of the current I. Contribution of the vortex dynamics on the voltage is reduced by a pinning potential or a defect by the resisting of the vortex movement which exist in this phase. Furthermore, the voltage increases abruptly at a certain value of the current I. It is occured because of the majority of the vortex movement in this phase cannot be resisted by a pinning potential or a defect. Beside of that, the current I passed to a clean superconductor with no external magnetic field can generate vortex-antivortex (VAV). The V-I curve for this phase has a same pattern with the V-I curve for a superconductor with a pinning potential or a defect (Machida and Kaburaki, 1993). A voltage curve as a function of time $V(t)$ relating the V-I curve and the vortex dynamics produces a sharp pulses when a number of vortex annihilate each other.

The numerical studies have explained the influence of vortex dynamics on the V-I curve. However, several fundamental questions, in particular, the influence of the annihilation dynamics of a VAV pair on the $V(t)$ curve remain open. This study is based on the numerical solution of the TDGL equations. The model is possible to visualize the annihilation dynamics of a VAV pair. Vortex or antivortex can be identified through a vector field of the supercurrent density $\mathbf{J}_s$ and the local magnetic induced $\mathbf{h} = \nabla\times\mathbf{A}$ where $\mathbf{A}$ is the magnetic vector potential. The influence of the annihilation dynamics of a VAV pair on the $V(t)$ curve can be found through the velocity curve as a function of time and the Cooper pairs density n_s.

2. Model

2.1 Ginzburg-Landau Superconductivity

In the Ginzburg-Landau model, a superconducting state of a sample is described by the free energy as a functional of the order parameter $\Psi = (n_s)^{1/2}\exp(i\theta)$, where θ is the phase of the order parameter. The Ginzburg-Landau's free energy density g_s is expressed as

$$g_s - f_n = -|\alpha(T)||\Psi|^2 + \frac{1}{2}\beta|\Psi|^4 + \frac{\hbar^2}{2m_s}\left|\left(\nabla - i\frac{e_s}{\hbar}\mathbf{A}\right)\Psi\right|^2 + \frac{1}{2\mu_0}\left|\mathbf{h} - \mu_0\mathbf{H}\right|^2 \quad (1)$$

where f_n is the free energy density for a normal phase, $i = \sqrt{-1}$, $e_s(=2e)$ and $m_s(=2m_e)$ are the effective charge and the effective mass of the Cooper pairs, μ_0 is the permeability of the free space, $\hbar$ is the Planck constant h divided by 2π, $\mathbf{H}$ is the external magnetic field, $|\alpha(T)|$ and β are phenomenological constants of the Landau's free energy density. The expression for $|\alpha(T)|$ as a function of temperature T is given by relation $|\alpha(T)| = |\alpha(0)|(1-T/T_c)$ where T_c is the critical temperature for a sample, phenomenological constant at zero temperature $|\alpha(0)| = \mu_0 H_{c2}(0)(\hbar e_s/2m_s) = (\Phi_0/2\pi\xi_{GL}(0))(\hbar e_s/2m_s)$ where $\Phi_0 = 2\pi\hbar/e_s$ is the flux quantum, $H_{c2}(0)$ is the second critical magnetic field at zero temperature, and $\xi_{GL}(0)$ is the coherent length at zero temperature. The relation of

$|\alpha(0)|$ and β is given by $\Psi^2_{\infty,\mathrm{GL}}(0) = 2\Psi^2_{\infty}(0) = |\alpha(0)|/\beta$. As an external parameter is applied on a superconductor, such as the external current density $\mathbf{J}_\mathrm{e}$, the superconductor will undergo a phase transition to the equilibrium states by the arranging of the order parameter in order to obtain a minimum free energy. The order parameter for this state is a solution of the TDGL equations, (Winiecki and Adam, 2002; Sato and Kato, 2007)

$$\frac{\hbar^2}{2m_\mathrm{s}D}\left(\frac{\partial}{\partial t}+\mathrm{i}\frac{e_s}{\hbar}\Phi\right)\Psi=\frac{\hbar^2}{2m_\mathrm{s}}\left(\nabla-\mathrm{i}\frac{e_s}{\hbar}\mathbf{A}\right)^2\Psi+\left(|\alpha(T)|-\beta|\Psi|^2\right)\Psi\ , \tag{2}$$

$$\nabla\times\left(\nabla\times\mathbf{A}-\mu_0\mathbf{H}\right)=\mu_0\mathbf{J}\ , \tag{3}$$

where D is a phenomenological diffusion constant. Eq. (2) is the Maxwell equation for the magnetic field, where the displacement current $\varepsilon_0\partial_t\mathbf{E}$ has been neglected. The total current $\mathbf{J}$ is given by the sum of the supercurrent density $\mathbf{J}_\mathrm{s}$ and the normal current density $\mathbf{J}_\mathrm{n}$. The expression of the supercurrent density is given by $\mathbf{J}_\mathrm{s} = (e_s\hbar/2m_\mathrm{s}\mathrm{i})(\Psi^*\nabla\Psi - \Psi\nabla\Psi^*) - (e_\mathrm{s}^2|\Psi|^2/m_\mathrm{s})\mathbf{A}$ which can be expressed in the form of $\mathbf{J}_\mathrm{s} = e_\mathrm{s}n_\mathrm{s}\mathbf{v}_\mathrm{s}$ where the velocity and the momentum of the effective charge of the Cooper pairs are $\mathbf{v}_\mathrm{s} = \mathbf{p}_\mathrm{s}/m_\mathrm{s}$ and $\mathbf{p}_\mathrm{s} = \hbar\nabla\theta - e_\mathrm{s}\mathbf{A}$. Symbol * indicates the conjugate complex. The normal current density is given by Ohm's law, $\mathbf{J}_\mathrm{n} = \sigma(-\nabla\Phi-\partial_t\mathbf{A}) = \sigma\mathbf{E}$, where Φ is the electric potential, $\mathbf{E}$ is the electric field and σ is the electric conductivity. The normal current density represents uncondensate electron in a superconductor.

The dimensionless forms of the Eq. (2) and (3) are (Winiecki and Adam, 2002)

$$(\partial_t\Psi + \mathrm{i}\Phi)\Psi = (\nabla - \mathrm{i}\mathbf{A})^2\Psi + (1-T)(1-|\Psi|^2)\Psi \tag{4}$$

$$\kappa^2\nabla\times\nabla\times\mathbf{A} = (1-T)(\nabla\theta-\mathbf{A})|\Psi|^2 + \sigma(-\nabla\Phi - \partial_t\mathbf{A}) + \kappa^2\nabla\times\mathbf{H}. \tag{5}$$

Lengths have been scaled in units of $\xi_\mathrm{GL}(0)$, time in unit of $\tau = \xi^2_\mathrm{GL}(0)/D$, Ψ in unit of $\Psi_{0,\mathrm{GL}}(0)(1-T)^{1/2}$, $\mathbf{A}$ in unit of $\Phi_0/2\pi\xi_\mathrm{GL}(0)$, $\mathbf{B}$ in unit of $\Phi_0/2\pi\,\xi^2_\mathrm{GL}(0)$, Φ in unit of $D\Phi_0/2\pi\,\xi^2_\mathrm{GL}(0)$, $\mathbf{H}$ in unit of $H_{c2}(0)$, $\mathbf{E}$ in unit of $D\Phi_0/2\pi\,\xi^3_\mathrm{GL}(0)$, σ in unit of $\sigma_0 = 1/\mu_0D\kappa^2$, T in unit of T_c, $\mathbf{J}$ in unit of $J_0 = H_{c2}(0)/\xi_\mathrm{GL}(0)$. The last term in Eq. (5) is the external current density, $\mathbf{J}_\mathrm{e} = \kappa^2\nabla\times\mathbf{H}$ where $\kappa=\lambda/\xi$ is the Ginzburg-Landau parameter.

The physical quantities $\mathbf{E}$, $\mathbf{B}$, $\mathbf{J}$, $|\Psi|^2$ are invariant under the transformation of $(\Psi, \mathbf{A}, \Phi) \rightarrow (\Psi\mathrm{e}^{\mathrm{i}\chi}, \mathbf{A} + \nabla\chi, \Phi - \partial_t\chi)$ where χ is an arbitrary scalar field. The potential gauge is chosen equal to zero, $\Phi - \partial_t\chi = 0$, in other word, $\Phi = 0$ at all times. This choice reduces Eq. (3) and (4) become

$$\partial_t\Psi = (\nabla - \mathrm{i}\mathbf{A})^2\Psi + (1-T)(1-|\Psi|^2)\Psi \tag{6}$$

$$\sigma\partial_t\mathbf{A} = (1-T)(\nabla\theta-\mathbf{A})|\Psi|^2 - \kappa^2\nabla\times(\nabla\times\mathbf{A}-\mathbf{H}) \tag{7}$$

2.2 Model System

The model system used is as follows. A type-II superconductor sized $8\xi_\mathrm{GL}(0)\times20\xi_\mathrm{GL}(0)$ with $\kappa = 1.3$ (niobium), $\sigma = 1$ and $T = 0$ is placed in a vacuum space without external magnetic field, Fig. 1(a). This situation gives boundary condition for Ψ in the form $(\nabla - \mathrm{i}\mathbf{A})|_\mathrm{n} = 0$. The external current density $\mathbf{J}_\mathrm{e} = J_{\mathrm{e};x}\hat{\mathbf{i}}$ is passed on the superconductor by imposing an external magnetic field difference between the upper and lower boundaries (Machida and Kaburaki, 1993; Vodolazov and Peeters, 2007). The last term in Eq. (5) gives $J_{\mathrm{e};x} = \kappa^2\,\partial_y H_z$ or in integral form become $\int_0^{L_y} J_{\mathrm{e};x}\,\mathrm{d}x = \kappa^2\int_{H_z}^{H_z}\mathrm{d}H_z$. The current-induced magnetic field at the upper and lower boundaries is given by $\mathbf{H}_\mathrm{t} = H_z\hat{\mathbf{k}} = J_{\mathrm{e};x}L_y/(2\kappa^2)\hat{\mathbf{k}}$ and $\mathbf{H}_\mathrm{b} = -\mathbf{H}_\mathrm{t}$. This condition gives boundary conditions for $\mathbf{A}$, namely $\nabla\times\mathbf{A} = \mathbf{H}$ with $\mathbf{H} = 0$ at $x = 0$ and $x = L_x$, $\mathbf{H} = \mathbf{H}_\mathrm{t}$ at $y = 0$, and $\mathbf{H} = \mathbf{H}_\mathrm{b}$ at $y = L_y$. This way reduces Eq. (6) become

$$\partial_t\mathbf{A} = (1-T)(\nabla\theta-\mathbf{A})|\Psi|^2 - \kappa^2\nabla\times\nabla\times\mathbf{A} \tag{8}$$

The voltage difference between $x = 0$ and $x = L_x$ caused by the VAV dynamics is calculated using $V(t) = \int_0^{L_x}\left[(1/L_y)\int_0^{L_y}(-\mathrm{d}\mathbf{A}/\mathrm{d}t)\,\mathrm{d}y\right]\mathrm{d}x$ (Machida and Kaburaki, 1994).

3. Method

The size of computational grid is chosen $N_x \times N_y = 80 \times 200$ where the size of the typical grid cell is $h_x \times h_y = 0.1\xi_\mathrm{GL}(0) \times 0.1\xi_\mathrm{GL}(0)$, see Fig. 1(b). The implication, the physical quantities become $x = \{x_i = (i-1)h_x: i=1,\ldots,N_x+1\}$, $y = \{y_j = (j-1)h_y : j = 1,\ldots,N_y+1\}$, $\Psi = \{\Psi_{i,j} : i = 1,\ldots,N_x+1; j = 1,\ldots,N_y+1\}$,

$A_x = \{A_{x;i,j} : i = 1,\ldots, N_x; j = 1,\ldots, N_y + 1\}$, $A_y = \{A_{y;i,j} : i = 1,\ldots, N_x + 1; j = 1,\ldots, N_y\}$, $B_z = \{B_{z;i,j} : i=1, \ldots, N_x; j=1, \ldots, N_y\}$. The evaluation points for Ψ, A_x, A_y, B_z at a typical grid cell (x_i, y_j) are shown at Fig. 2(b).

The TDGL equations are discretized using the finite difference method where the Euler method is used to discretize time variable. U-Ψ method (Gropp et al., 1996) is used to preserve gauge invariance under discretization with the link variables $U_{\mu;i,j} = \exp(-\mathrm{i} A_{\mu;i,j} h_\mu)$ for $\mu = x, y$ (Barba-Ortega et al., 2010; Bolech et al., 1995; Kaper and Kwong, 1995; Sardella et al., 2006; Vodolazov et al., 2003). The discrete forms of Eq. (6) and (8) are $\Psi_{i,j}^{n+1} = \Psi_{i,j}^{n} + \Delta t \partial_t \Psi_{i,j}^{n}$ for $i = 2, \ldots, N_x, j = 2, \ldots, N_y$; $A_{x;i,j}^{n+1} = A_{x;i,j}^{n} + \Delta t \partial_t A_{x;i,j}^{n}$ for $i = 1, \ldots, N_x, j = 2, \ldots, N_y$ and $A_{y;i,j}^{n+1} = A_{y;i,j}^{n} + \Delta t \partial_t A_{y;i,j}^{n}$ for $i = 2, \ldots, N_x, j = 1, \ldots, N_y$ where

$$\partial_t \Psi_{i,j} = \frac{U_{x;i-1,j}^{*} \Psi_{i-1,j} - 2\Psi_{i,j} + U_{x;i,j} \Psi_{i+1,j}}{h_x^2} + \frac{U_{x;i,j-1}^{*} \Psi_{i,j-1} - 2\Psi_{i,j} + U_{y;i,j} \Psi_{i,j+1}}{h_y^2} + (1-T)(1-|\Psi_{i,j}|^2)\Psi_{i,j}$$

$$\partial_t A_{x;i,j} = \frac{(1-T)\,\mathrm{Im}(U_{x;i,j} \Psi_{i,j}^{*} \Psi_{i+1,j})}{h_x} - \kappa^2 \frac{(A_{y;i+1,j} - A_{y;i,j} - A_{y;i+1,j-1} + A_{y;i,j-1})}{h_x h_y} + \kappa^2 \frac{(A_{x;i,j+1} - 2A_{x;i,j} + A_{x;i,j-1})}{h_y^2}$$

$$\partial_t A_{y;i,j} = \frac{(1-T)\,\mathrm{Im}(U_{y;i,j} \Psi_{i,j}^{*} \Psi_{i,j+1})}{h_y} - \kappa^2 \frac{(A_{x;i,j+1} - A_{x;i,j} - A_{x;i-1,j+1} + A_{y;i-1,j})}{h_x h_y} + \kappa^2 \frac{(A_{y;i+1,j} - 2A_{y;i,j} + A_{y;i-1,j})}{h_y^2}$$

Im indicates imaginary part. In this simulation, $\Delta t = 0.001\,\tau$ is chosen to fill a stability criterion, $\Delta t < (h_x)^2/2\kappa^2$ where $h_x = h_y$ (Winiecki and Adam, 2002a). The boundary conditions for Ψ at $y = y_1, y_{Ny+1}$ and $x = x_1, x_{Nx+1}$ are $\Psi_{1,j} = U_{x;1,j} \Psi_{2,j}$, $\Psi_{Nx+1,j} = U_{x;Nx,j}^{*} \Psi_{i+1,j}$, $\Psi_{i,1} = U_{x;i,1} \Psi_{i,2}$, $\Psi_{i,\,Ny+1} = U_{y;i,Ny}^{*}\ \Psi_{i,j+1}$. The order parameters at the corners are evaluated using average of the two nearest neighbors. The boundary conditions for **A** at $y = y_1, y_{Ny+1}$ and $x = x_1, x_{Nx+1}$ are $A_{x;i,1} = -h_y (h_x)^{-1}(A_{y;i+1,1} - A_{y;i,1}) + A_{x;i,2} - h_y H_z$, $A_{x;i,Ny+1} = h_y (h_x)^{-1}(A_{y;i+1,Ny} - A_{y;i,Ny}) + A_{x;i,Ny} - h_y H_z$, $A_{y;1,j} = -h_x (h_y)^{-1}(A_{x;1,j+1} - A_{x;1,j}) + A_{y;2,j}$, $A_{y;Nx+1,j} = h_x (h_y)^{-1}(A_{x;Nx,j+1,} - A_{x;Nx,j}) + A_{y;Nx,j}$.

The voltage is calculated using

$$V = \frac{L_x}{N_x N_y} \sum_{j=1+a}^{N_y - a} \sum_{i=1+a}^{N_x - a} \frac{1}{3} \left\{ \sqrt{\left(\frac{\mathrm{d}A_{x;i,j}}{\mathrm{d}t}\right)^2 + \left(\frac{\mathrm{d}A_{y;i,j}}{\mathrm{d}t}\right)^2} + \sqrt{\left(\frac{\mathrm{d}A_{x;i,j+1}}{\mathrm{d}t}\right)^2 + \left(\frac{\mathrm{d}A_{y;i,j}}{\mathrm{d}t}\right)^2} + \sqrt{\left(\frac{\mathrm{d}A_{x;i,j}}{\mathrm{d}t}\right)^2 + \left(\frac{\mathrm{d}A_{y;i+1,j}}{\mathrm{d}t}\right)^2} \right\}$$

where a = 0, 1, 2, …. The sample size in the model system is relatively small so that the surface effects tend to dominate. In order to remove the surface effects from the V calculation, it is used a =13 which gives $l = a h_x = \kappa \xi_{GL}(0) = \lambda_{GL}(0)$ measured from boundaries.

4. Result and Discussion

4.1 Vortex-Antivortex Determination

The annihilation dynamics of a VAV pair occurs when $J_{e;x} = 0.12\, J_0$ is passed on the superconductor. The vortex or antivortex is known from the physical quantities n_s, $\mathbf{J}_s$ and B_z. Fig. 2 shows that the vortex and antivortex have the same n_s curve so the vortex or antivortex cannot be determined from the n_s curve. Moreover, $\mathbf{J}_s$ keeps the vortex and antivortex remain localized in the sample. The $\mathbf{J}_s$ circulations for the vortex and antivortex have the opposite direction. These directions are related to the direction of the quantum of magnetic flux or induction (flux quantum). $\mathbf{J}_s$ clockwise will keep the flux quantum localized at $-z$ axis direction as antivortex, namely $\mathbf{B}_{AV} = -\Phi_0 \hat{\mathbf{k}}$, and $\mathbf{J}_s$ counter clockwise will keep the flux quantum localized at $+z$ axis direction as vortex, namely $\mathbf{B}_V = \Phi_0 \hat{\mathbf{k}}$. The indexes of the AV and V are abbreviated for Anti Vortex and Vortex. $\mathbf{J}_s$ also acts as the screening currents for a homogeneous external magnetic field. Fig. 3 shows that $|\mathbf{J}_s|$ at the edges of the sample subjected to the current-induced magnetic field is greater than $|\mathbf{J}_s|$ inside the material. $|\mathbf{J}_s|$ is zero at the center of vortex and anti-vortex.

4.2 Annihilation Dynamics of a VAV Pair

The curves of the position, velocity and acceleration of the VAV pair for $J_{e;x} = 0.12 J_0$ are shown in Fig. 3.a. The position curves can be represented by the equations of $y_{AV} = 5{\cdot}10^{-12}t^6 + 4{\cdot}10^{-10}t^5 - 10^{-6}t^4 + 3{\cdot}10^{-4}t^3 - 0.036t^2 + 2.0196t - 39.225$ and $y_V = -y_{AV}$ with $R^2 = 0.9944$ for $40.1\,\tau \le t \le 172.2\,\tau$. The first and second derivation result the equations of the speed and acceleration, namely $v_V = 3{\cdot}10^{-11}t^5 - 4{\cdot}10^{-6}t^3 + 9{\cdot}10^{-4}t^2 - 0.0728t + 2.0196$ in unit of $\xi_{GL}(0)\,\tau^{-1}$ and $a_V = 3{\cdot}10^{-11}t^5 - 4{\cdot}10^{-6}t^3 + 9{\cdot}10^{-4}t^2 - 0.0728$ in unit of $\xi_{GL}(0)\,\tau^{-2}$, Fig. 3.b and 3.c. The pair

penetrate inside the sample at $t = 40.1\,\tau$ with the same speed, namely $v_0 = 2.0196\xi_{GL}(0)\tau^{-1}$. The pair has the decreasing of the speed at $t < 68\,\tau$, the minimum speed at $t = 68\,\tau$, and the increasing of the speed at $68\,\tau < t < 172.2\,\tau$. Finally, the vortex and antivortex annihilate each other in the centre of the sample at $t = 172.2\,\tau$ with the maximum speed. The annihilation occurs periodically.

It is clear that there is a force moving of the vortex and antivortex. The external current density $\mathbf{J}_e$ causes that the force density of $\mathbf{F}_{AV} = \mathbf{J}_e \times \mathbf{B}_V = J_{e,x}\Phi_0\,\hat{\mathbf{j}}$ and $\mathbf{F}_V = -\mathbf{F}_{AV}$ respectively work on the antivortex and the vortex (Tinkham, 1996). These force drive them toward the centre of the sample with velocity $\mathbf{v}_{AV} = v_{AV}\,\hat{\mathbf{j}}$ for the antivortex and $\mathbf{v}_V = -v_V\,\hat{\mathbf{j}}$ for the vortex. The VAV in motion creates an electric field $\mathbf{E} = \mathbf{B} \times \mathbf{v}$ which is parallel to $\mathbf{J}_e$. The electric fields cause $\mathbf{J}_e$ dissipate energy $\mathbf{E} \bullet \mathbf{J}_e$ and generate the resistive voltage $V = EL_x = B_z v L_x$ where $v = v_{AV} = v_V$.

4.3 Voltage Curve

Fig. 4.a shows the voltage curve of the annihilation dynamics of a VAV pair for $J_{e,x} = 0.12J_0$. It appears two types of pulse, i.e. the sharp pulse and the small pulse. The small pulses (A_1, A_2, A_3 in Fig 4.a) appear periodically when the vortex and antivortex penetrate in the sample, namely at $t = 45.1\,\tau$, $196.3\,\tau$, $347.6\,\tau$. The sharp pulses (C_1, C_2, C_3 in Fig. 4.a) appear periodically when the annihilations of a VAV pair are occurred, i.e. at $t = 172.2\,\tau$, $323.5\,\tau$, $474.7\,\tau$. The two types of pulse have the same period, namely $\Theta = 151.25\,\tau$. The relation $V = B_z v L_x$ shows that the maximum speeds of the vortex and antivortex as they annihilate are a cause of the appearance of the sharp pulses. It seems that the small pulses characterize the penetrating of the vortex and antivortex into the sample and the sharp pulses characterize the annihilation of a VAV pair.

Fig. 4.b shows the voltage curve for $J_{e,x} = 0.13J_0$. The voltage curve has the same pattern as before. The difference is that it appears two small pulses, A and B1, before the first sharp pulse C1. It means that there are two pairs of VAV before the annihilation a VAV pair. In addition, the two types of pulse have a shorter period than before.

5. Conclusion

The influence of the annihilation a pair of VAV has been studied based on the TDGL model. The small pulses on the voltage curve characterize the vortex and anti-vortex penetrates into a sample. The sharp pulses characterize the phenomenon of annihilation a pair of VAV. The periodicity of the pulses decreases by the increasing of the external current density.

Acknowledgements

Thanks to the DIKTI that has provided assistance in the form of scholarships BPPS during the study.

References

Barba-Ortega, J., Becerra, A., Aguiar, J.A. (2010). Two Dimensional Vortex Structures in a Superconductor Slab at Low Temperatures, *Physica C*, 470, 225-230

Bolech, C., Buscaglia, G.C., Lopez, A. (1995). Numerical Simulation of Vortex Arrays in Thin Superconducting Films, *Physical Review B*, 52, 22, R15719-R15722

Gropp, W.D., Kaper, H.G., Leaf, G.K., Levine, D.M., Palumbo, M., Vinokur, V.M. (1996). Numerical Simulation of Vortex Dynamics in Type-II Superconductors, *Journal of Computational Physics*, 123, 254-266

Kaper, H.G and Kwong M.K. (1995). Vortex Configurations in Type-II Superconducting Films, Journal of Computational Physics, 119, 120-131

Machida, M. and Kaburaki, H. (1993). Direct simulation of the Time Dependent Ginzburg-Landau Equation for Type II Superconducting Thin Film: Vortex Dynamics and V-I Characteristics, *Physical Review Letter*, 71, 3206-3209

Machida, M. and Kaburaki, H. (1994). Numerical simulation of flux-pinning dynamics for a defect in a type-II superconductor. *Physical Review B*, 50, 2, 1286-1289

Winiecki, T. and Adam, C.S. (2002a). A Fast Semi-Implicit Finite-Difference Method for the TDGL Equations. *Journal of Computational Physics*, 179, 127-139

Winiecki, T. and Adam, C.S. (2002b). Time-dependent Ginzburg-Landau simulation of the voltage-current characteristic of type-II superconductors with pinning. *Physical Review B*, 65, 104517

Sardella, E., Malvezzi, A.L., Lisboa-Filho, P.N. (2006). Temperature-dependent Vortex Motion in a Square Mesoscopic Superconducting Cylinder: Ginzburg-Landau Calculations, *Physical Review B*, 74, 014512

Sato, O. and Kato, M. (2007). Penetrations and dynamics of vortices in mesoscopic superconducting plate. *Physica C*, 463-465, 258-262

Tinkham, M. (1996). *Introduction to Superconductivity*. New York: McGraw-Hill, Inc., p. 164

Vodolazov, D.Y., Maksimov, I.L., Brandt, E.H. (2003). Vortex Entry Conditions in Type-II Superconductors. Effect of Surface Defects, *Physica C*, 384, 211-226
Vodolazov, D.Y., Peeters, F.M. (2007). Rearrangement of the vortex lattice due to instabilities of vortex flow. *Physical Review B*, 76, 014521

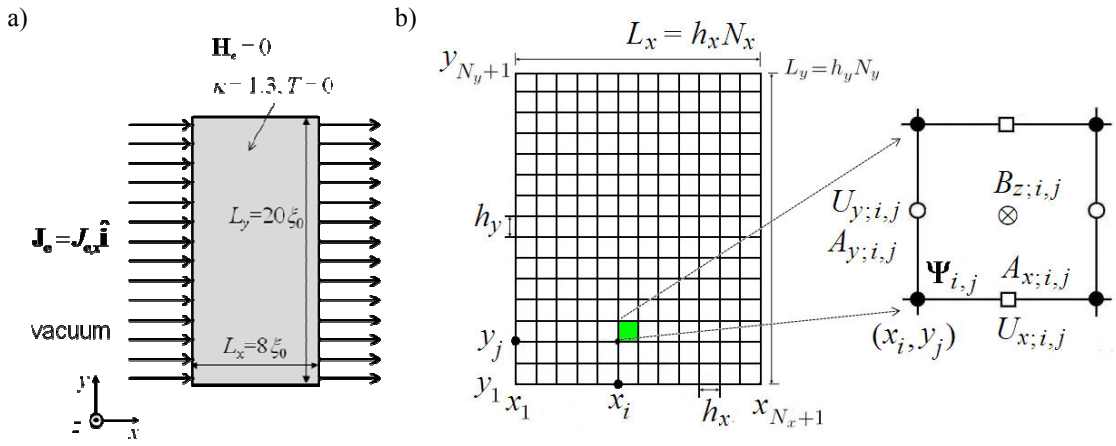

Figure 1. (a) Model system, (b) computational grid and typical grid cell at (x_i, y_j) for $\Psi_{i,j} = \Psi(x_i, y_j)$, $A_{x;i,j} = A_x(x_i + 0.5h_x, y_j)$, $A_{y;i,j} = A_y(x_i, y_j + 0.5h_y)$, $B_{z;i,j} = B_z(x_i + 0.5h_x, y_j + 0.5h_y)$

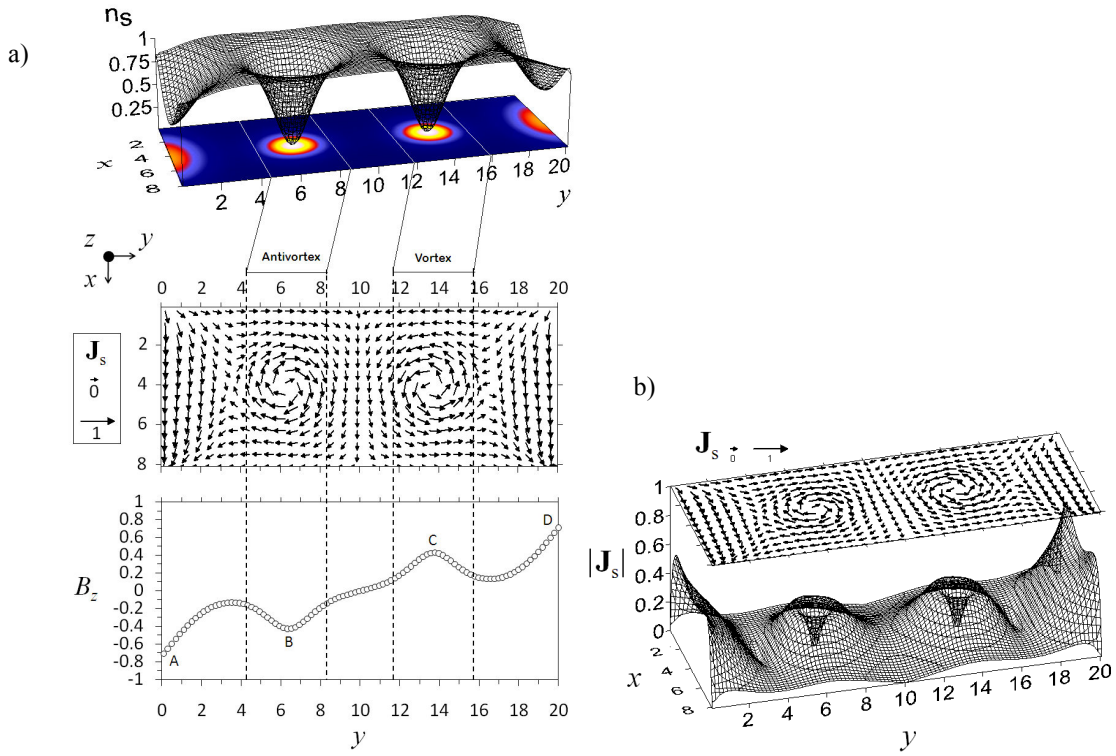

Figure 2. (a) Snapshot for n_s density (top), supercurrent density $\mathbf{J}_s$ (midle) and magnetic field induction B_z (bottom) at $t = 120\tau$. (b) Snapshot for contour and vector field of supercurrent density $\mathbf{J}_s$ at $t = 120\tau$.

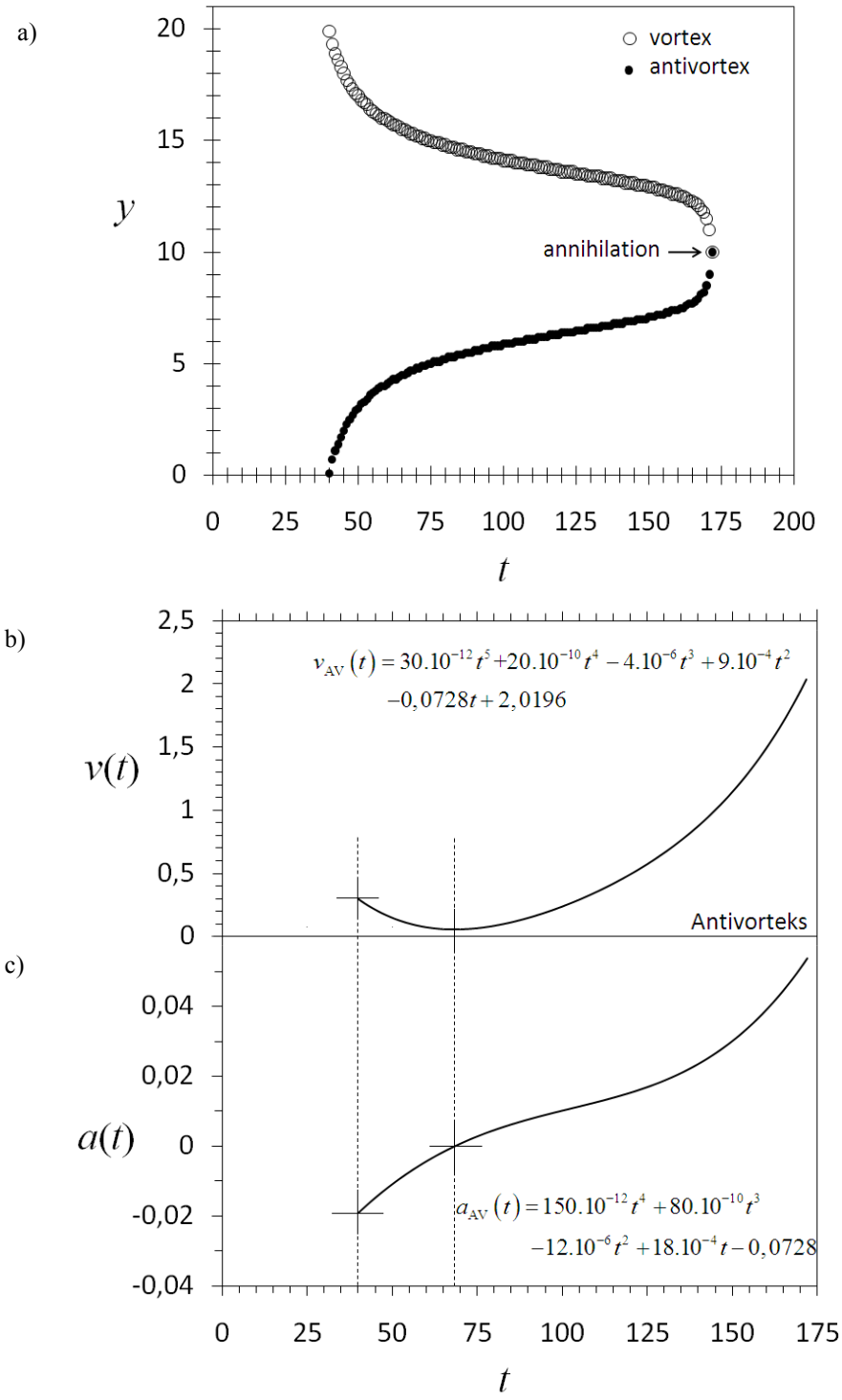

Figure 3. Position, velocity and acceleration as a function of time for the VAV dynamics for $J_e = 0.12\ J_0$

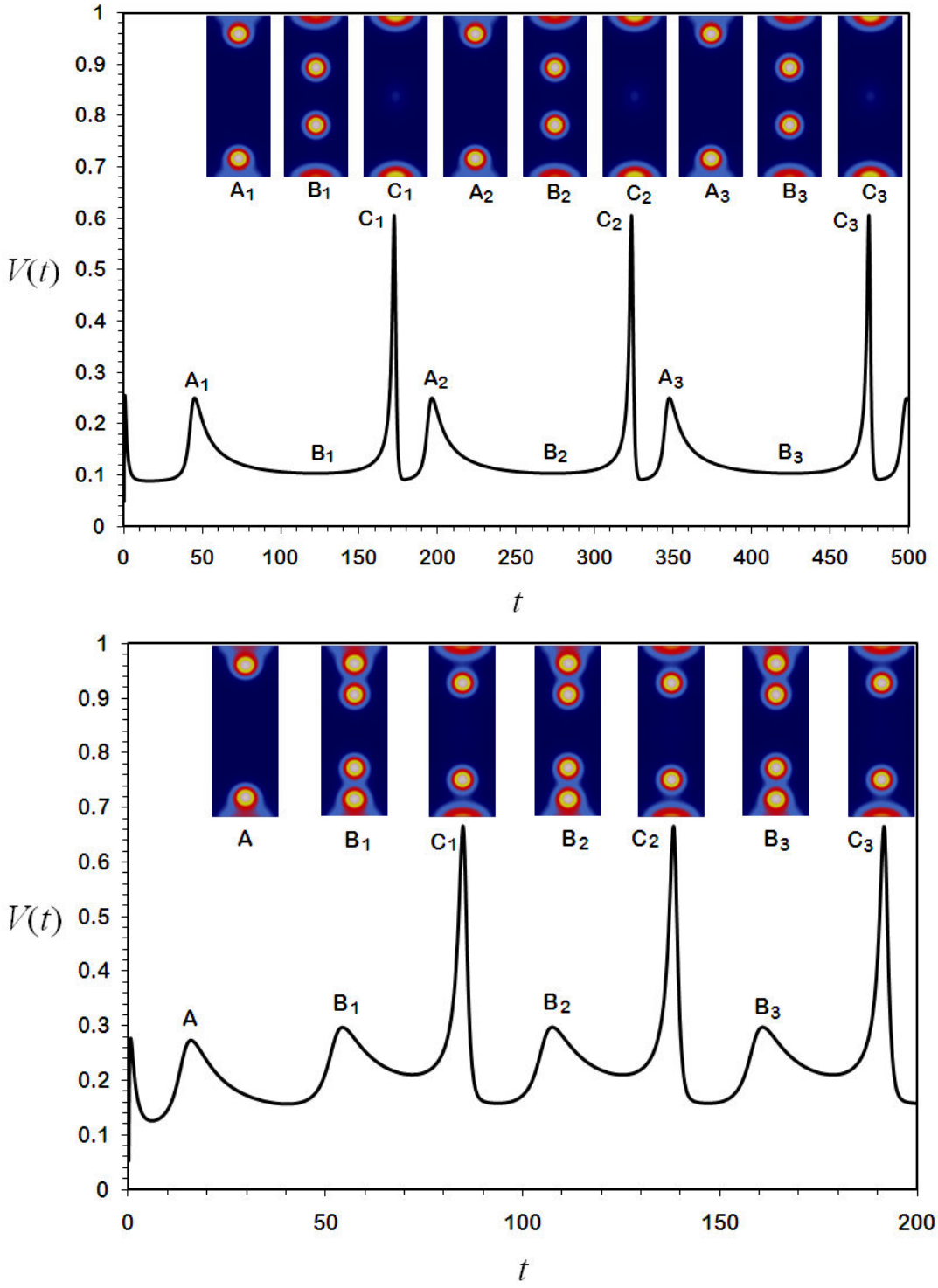

Figure 4. Voltage curve as a function of time of the annihilation dynamics of a VAV pair for (a) $J_e = 0.12\ J_0$ and (b) $J_e = 0.13\ J_0$ where t in unit of $\tau = \xi^2_{GL}(0)/D$, V in unit of $D\Phi_0/2\pi\,\xi^3_{GL}(0)$